Lab on a Chip

COMMUNICATION

View Article Online
View Journal | View Issue

Cite this: *Lab Chip*, 2025, **25**, 2320

Received 30th January 2025,
Accepted 2nd April 2025

DOI: 10.1039/d5lc00105f

rsc.li/loc

Calcite-functionalized microfluidic chip for pore scale investigation of biogeochemical interactions in porous media†

Na Liu*[a] and Martin A. Fernø [ab]

Micromodels are widely used to simulate subsurface reservoir environments for investigating multiphase flow and interactions within porous media. However, existing models often fail to accurately replicate the geochemical characteristics of reservoir minerals due to material limitations. This study presents a method for fabricating calcite-functionalized micromodels, wherein calcite crystals are grown *in situ* through microbial-induced carbonate precipitation (MICP). The technique enables precise, site-selective calcite growth, offering control over the morphology of $CaCO_3$ precipitates, as well as the geometry and porosity of the micromodels. The resulting calcite-functionalized micromodels more accurately mimic the mineralogical and physical properties of natural carbonate reservoirs. Utilizing these micromodels, we achieved real-time visualization of geochemical and biogeochemical processes within porous media, facilitating detailed examination of pore-scale microbial-fluid–rock interactions pertinent to gas storage applications.

Introduction

Microfluidic pore networks, commonly referred to as micromodels, are artificial, quasi two-dimensional porous media that enable direct visualization of complex flow environments in porous media.[1,2] In recent years, micromodels have become valuable tools for studying multiphase fluid flow and gas, rock, and liquid interactions in subsurface reservoirs.[3] Advanced fabrication methods, such as top-down etching or lithographic techniques, have been employed to accurately replicate the geometric pores of real rock samples.[4–6] These micromodels can be precisely engineered to control key porous media properties such as porosity, permeability, and wettability. Most micromodels constructed to date, however, use materials such as silicon,[7] glass,[8] and polymers,[9] rather than actual rock. Reliance on non-representative materials limits the parameter space of investigation, in particular in the bio-geochemical context and mineral dissolution/precipitation. To avoid limitation of variables or conditions that are being studied or analyzed, micromodels should incorporate and accurately replicate the native chemical, physical, and biological conditions of subsurface environments.

Of particular interest with respect to carbonate reservoirs are the effects of carbonate dissolution and precipitation during biogeochemical interactions.[10] Emerging techniques have enabled the partial or complete conversion of glass and silicon surfaces to calcite in microfluidic channels or pore networks by coating,[11] photolithographic,[12] packing[13] or 3D printing[14] techniques. A rigorous investigation of the parameters that affect the polymorphic composition, morphology, and distribution of $CaCO_3$ coating on functionalized silicon surfaces is, however, not available in the literature. Additionally, materials and adhesives commonly used during surface coating can introduce contaminants into the pore network, potentially altering geochemical reactions, particularly in microbial studies.[15] Developing a simple and controllable method for fabricating site-selective, *in situ* grown calcite-functionalized micromodels is therefore essential. Such micromodels would combine the precise engineering capabilities of silicon and glass substrates with the chemical authenticity of carbonate materials. Song *et al.*[16] developed a carbonate-functionalized microfluidic device to investigate calcite dissolution during CO_2 injection within a single pore. Building on this, our study advances the field by introducing kinetic control over the calcite precipitation process within a complex pore network. By optimizing geometry, porosity, and distribution of $CaCO_3$ precipitates in the pore network, these micromodels accurately replicate the physical and chemical properties of subsurface carbonate reservoirs, enabling the study of biogeochemical interactions under reservoir-relevant conditions while supporting microbial activity.

[a] *Department of Physics and Technology, University of Bergen, Norway. E-mail: Na.Liu@uib.no*
[b] *Norwegian Research Centre AS – NORCE, Norway*

† Electronic supplementary information (ESI) available. See DOI: https://doi.org/10.1039/d5lc00105f

Fabrication of calcite-functionalized micromodels

Achieving controllable *in situ* $CaCO_3$ growth in micromodels involves leveraging the microbial-induced carbonate precipitation process, which mimics the natural carbonate formation observed in reservoirs.[17] The pore network used here is etched in a silicon wafer (27 mm × 22 mm × 0.03 mm) using 36 (9 × 4) repetitions of a unique pore pattern of a natural sandstone, yielding a total porosity of 0.62 and pore volume of 11.1 μL.[18] The manufacturing procedure ensured strongly hydrophilic grain surfaces (100% pure quartz) with a 100 nm roughness, replicating realistic capillary forces in the pore network.[19] The pore network contains pores ranging in size from a few μm^2 to 10^4 μm^2, with an average size of 3896 μm^2, and grains ranging from a few μm^2 to 10^5 μm^2, averaging 6238 μm^2.[20]

The bacterium *Sporosarcina pasteurii* DSM 33 (DSMZ GmbH) was employed to produce urease, which hydrolyzes urea into ammonium (NH_4^+) and carbonate (CO_3^{2-}), increasing pH and alkalinity to promote $CaCO_3$ precipitation in the presence of calcium ions.[21] Following a 16 hour incubation in the pore network at 30 °C, 1.5 pore volume of cement solution (0.5 M $CaCl_2$ and urea) was injected to induce $CaCO_3$ precipitation. Extracellular polymeric substances (EPS) and suspended biomass provided negatively charged functional groups for cation adsorption, and served as nucleation sites for precipitation (Fig. 1). Raman spectroscopy confirmed calcite as the dominant crystalline phase after 20 hours of crystallization (Fig. S2†). Crystal pore occupancy was determined using a flow-based fluorescence (1500 ppm sodium fluorescein solution) approach to evaluate the vertical growth dimension. Estimates of porosity reduction only consider precipitates that occupy the entire pore depth (30 μm) and fully restrict flow. This stringent criterion, which excludes precipitates with partial vertical coverage, results in an underestimation of porosity reduction by up to 10%. The details of the image segmentation and porosity calculation can be found in the ESI† (Fig. S3). To mitigate unwanted inlet area pore clogging during cement solution injection (Fig. S4†), the microchip was immersed in a weak acid solution to effectively dissolve the obstructions while preserving most of the $CaCO_3$ precipitates within the pore network. The MICP process can be repeated to refine the geometry and porosity of the calcite-functionalized micromodel as needed. Further details on the experimental setup and procedure are provided in the ESI† (Fig. S1).

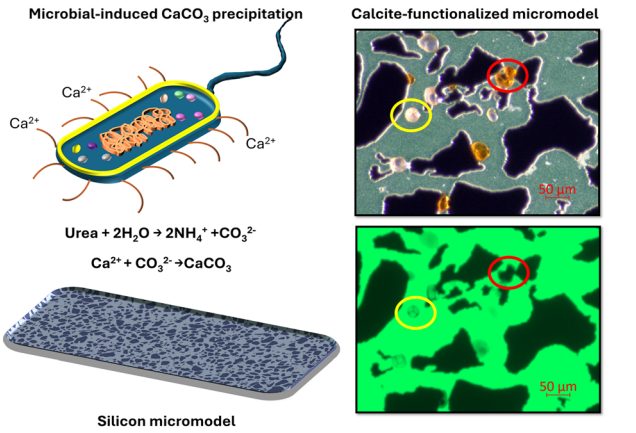

Fig. 1 Design and characterization of calcite-functionalized micromodels. This schematic illustration depicts the fabrication process of calcite-functionalized micromodels *via* microbial-induced carbonate precipitation. The right column shows microscopy images of deposited calcite precipitates within the pore network, captured in bright-field (top) and fluorescence (bottom) channels. Calcite precipitates are categorized into two types: partial growth that restricts flow (highlighted by yellow circles) and complete growth that blocks flow (indicated by red circles).

Tunable geometry and porosity

The MICP process allows for selective and controllable $CaCO_3$ growth and precipitation within the pore network, enabling micromodels to better represent the geochemical and geophysical properties of real carbonate rocks. This method is essential for precisely adjusting the geometry and porosity of micromodels, particularly at micrometer pore-length scales, which is challenging with conventional techniques (see Fig. S5†). Microbial activity and pore network hydrodynamics influence the kinetics of $CaCO_3$ nucleation and crystal growth during MICP. By manipulating these factors, spatial control over the biomineralization process can be achieved, affecting pore-scale properties of $CaCO_3$, such as crystal size and polymorphism.[22–25] Thus, the porosity and geometry of the calcite-functionalized micromodel can be adjusted by manipulating operational parameters like pressure and injection cycles (Fig. S6†). While the optimum temperature for the *Sporosarcina pasteurii* strain is 30 °C, temperature could also serve as an effective control parameter but was not included in this study.

The morphologies of the $CaCO_3$ forms can be controlled by adjusting the precipitation time. Initially, amorphous $CaCO_3$ (ACC, $CaCO_3{\cdot}nH_2O$) formed immediately upon contact of the two solutions. Over time, ACC dehydrates into crystalline $CaCO_3$ polymorphs, such as vaterite and calcite.[24] After one day, most of the precipitates transform into calcite (the most stable form). The wettability of the precipitated calcite is inherently hydrophilic (*cf.* Fig. S7†), as freshly formed calcite crystals exhibit natural hydrophilic properties.[26] During MICP, EPS and biomolecules from *Sporosarcina pasteurii* adsorb onto the calcite surface, enhancing its hydrophilicity through the presence of functional groups such as hydroxyl, carboxyl, and amine groups.[27] This process closely replicates the natural wettability characteristics of carbonate reservoirs, where water preferentially wets the rock surface. Below we describe the interplay between three operational parameters that

determine the precipitate size, number and spatial distribution that influence porosity reduction.

The crystallization process and the supersaturation state of the solution are strongly influenced by *pore pressure* – higher pressures promote larger precipitates at fewer nucleation sites, whereas lower pressures favour smaller precipitates. The number of deposited $CaCO_3$ precipitates is tuneable by applying a *multi-cycle cement solution injection* protocol.[28] Further, the spatial distribution of precipitates within the pore network is influenced by the local *flow velocity field*, where high-velocity regions enhance Ca^{2+} availability, resulting in growth of larger precipitates (Fig. 2). For the pressures studied in this work the largest porosity reduction was observed at 50 barg (Fig. S6a†), with large precipitates distributed in the pore network. A linear trend was observed for the reduction of porosity as a function of the number of injection cycles (Fig. S6b†), and the deposited precipitates altered the hydrodynamics of the pore space, where shift from high- to low-velocity zones extended $CaCO_3$ growth to other areas of the pore network over subsequent cycles.

By controlling the operational parameters (*i.e.*, pore pressure, precipitation time, injection cycles), we can create a pore network with tuneable geometry, porosity, and mineralogy. Next we describe one geochemical and one bio-geochemical application enabled by this calcite-functionalized micromodel.

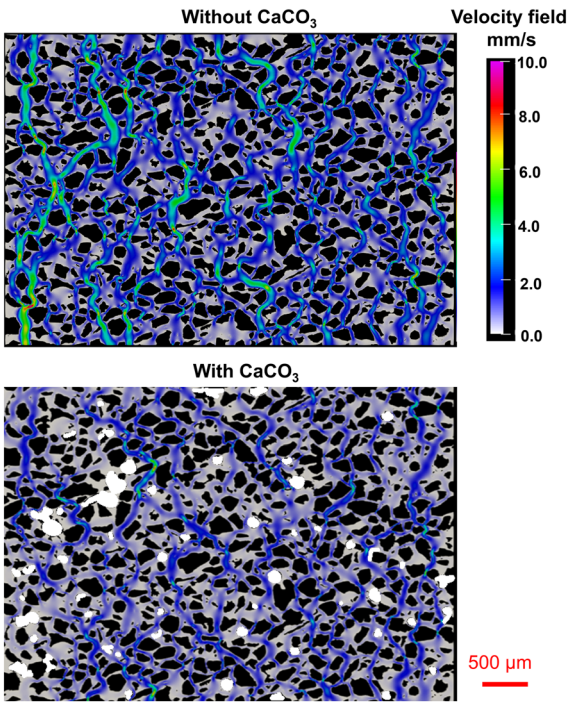

Fig. 2 Effects of crystal growth on the velocity field in the pore network. The top image shows the velocity field in the pore network without calcite crystals. The bottom image illustrates the reduced velocity field, both locally and globally, due to the deposition of calcite precipitates (white) predominantly in high-velocity zones. The velocity fields are generated with OpenFOAM.[29]

Example of geochemical processes

Geochemical reactions are particularly prone to occur during carbon storage in carbonate reservoirs, where the acidic CO_2-saturated brine may dissolve carbonaceous grains and surfaces. Understanding the mechanisms and dynamics of carbonate dissolution under reservoir conditions is crucial for evaluating the integrity and stability of reservoir rocks during carbon storage.[30] Pore-scale observations of carbonate dissolution kinetics and the interplay between CO_2 exsolution/mineralization and mineral dissolution/precipitation may be studied during supercritical CO_2 ($scCO_2$) injection using a calcite-functionalized, high-pressure micromodel (Fig. 3). The deposited precipitates were structurally stable for the pressure range applied (80–120 barg) before the dissolution process was initiated during $scCO_2$ injection. The $CaCO_3$ dissolution rate was determined by the reactive surface area, and the presence of a free CO_2 phase (injected or exsolved) impeded the dissolution rate by reducing the reactive surface area and blocking the mass transport in the interface.[16,23] To the best of our knowledge, this study presents the first pore-scale observation of combined calcite dissolution and precipitation occurring simultaneously within a functionalized micromodel.

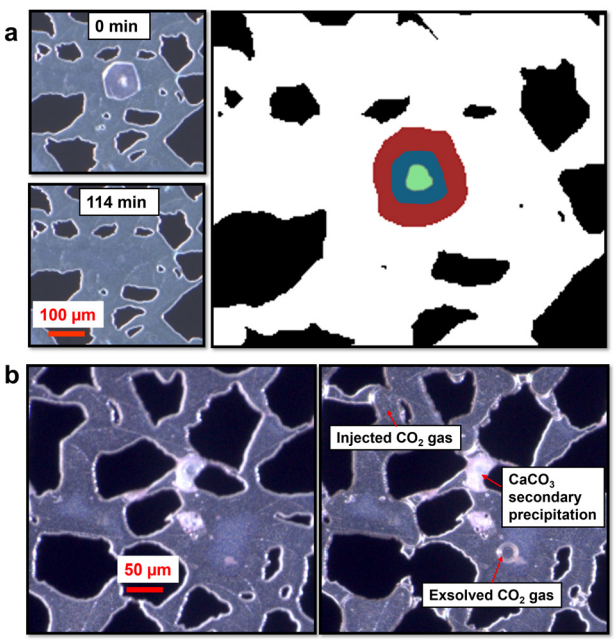

Fig. 3 Flow-induced carbonate dissolution and secondary $CaCO_3$ precipitation in a calcite-functionalized micromodel during $scCO_2$ injection. (a) The left images show microscope views of calcite dissolution. The right concept image uses brown to represent initial $CaCO_3$ precipitates, blue for after 1 hour, and green for after 1.5 hours in carbonated water (white) at 100 bar and 32 °C. Complete dissolution occurred within 2 hours. Time-lapsed images can be found in Fig. S8.† (b) Experimental observation of $CaCO_3$ dissolution and secondary precipitation during $scCO_2$ injection. The experimental procedure is detailed in the ESI.†

Example of bio-geochemical interactions

Underground porous media hydrogen storage is emerging as an option to balance the seasonal fluctuations in renewable energy supply and demand. However, potential microbial risks—such as microbial hydrogen consumption, changes in gas composition, clogging, and corrosion—underscore the need for effective monitoring and control of microbial activity in subsurface environments.[7,31] A key factor for successful underground hydrogen storage is understanding the interplay of bio-geochemical reactions occurring between microbes, fluids, rocks, and hydrogen gas under subsurface conditions. Here we present the first bio-geochemical interactions and hydrogen consumption in porous media (Fig. 4) using live microbial cells (hydrogenotrophic sulfate-reducing *DSM 17464 Oleidesulfovibrio alaskensis*) in a high-pressure, calcite-functionalized micromodel (100 barg). Pore-scale observations revealed that carbonate minerals do not react directly with hydrogen gas under a wide pressure range from 10 to 100 barg. This finding provides important data to a topic that is still debated in the literature.[32,33] However, carbonate minerals play a significant role in bio-geochemical interactions by buffering the aqueous phase, which in turn promotes increased microbial hydrogen consumption.

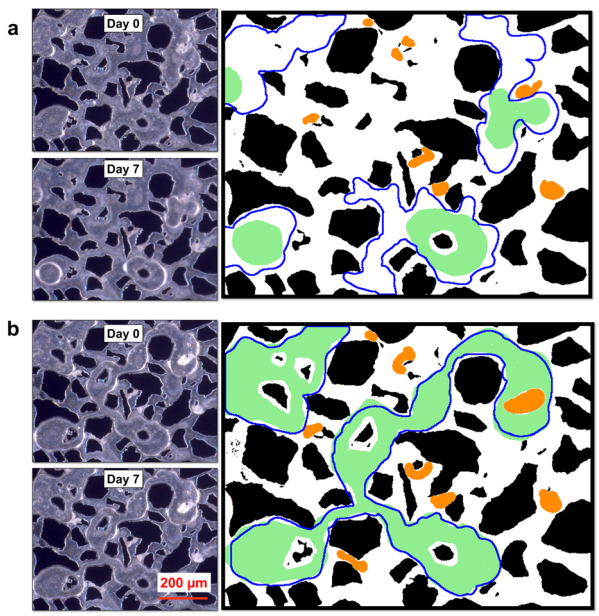

Fig. 4 Bio-geochemical interactions during porous media hydrogen storage. (a) *Microbial hydrogen consumption in a calcite-functionalized micromodel*: inoculated microbial cells utilized hydrogen gas as an electron source for sulfate reduction. Over the seven-day experiment, continuous microbial activity led to hydrogen gas consumption, with no observed changes in $CaCO_3$ precipitation. (b) *Interaction of calcite with pure hydrogen gas without microbes*: the interaction between hydrogen gas and calcite was studied under pressures ranging from 10 to 100 barg. Under these conditions, both the gas and calcite remained unchanged over time. The left column shows original microscopy images, whereas the right column presents conceptual representations (blue outlines: gas distribution at day 0; green: gas distribution at day 7, orange: calcite precipitates; black: grains; white: aqueous phase). Experimental conditions were P = 30 barg, T = 37.5 ± 0.5 °C. Details of the experimental procedure are provided in the ESI.†

Conclusions

The MICP-based mineral micromodel fabrication process allows for tailoring pore geometries and mineral compositions to suit specific experimental requirements, providing a customizable approach to studying diverse subsurface systems. The stability and performance of the calcite-functionalized micromodel was validated in studies on $scCO_2$ injection induced $CaCO_3$ dissolution (up to 120 barg) and microbial interactions with hydrogen gas. By replicating natural conditions while maintaining precise experimental control, calcite-functionalized microfluidic chips bridge the gap between laboratory studies and field-scale applications.

Beyond these applications, the capability of depositing other minerals (*e.g.*, sulfate minerals, pyrite) enables the creation of high-pressure multi-mineral micromodels. This significantly broadens the technology's potential for studying a wide range of geological and environmental processes under realistic reservoir conditions. Given these capabilities and demonstrated successes, we anticipate that calcite-functionalized microfluidic chips will play a transformative role in advancing research on biogeochemical processes in subsurface systems, with important implications for sustainable energy and environmental management.

Data availability

- Simulation data for this article are available at GitHub – **https://github.com/daavid00/pymm**: open-source image-based framework for computational fluid dynamics on microsystems.
- The data supporting this article have been included as part of the ESI.†

Author contributions

Na Liu: conceptualization, methodology, investigation, writing – original draft; Martin A. Fernø: data curation, supervision, funding acquisition, writing – original draft.

Conflicts of interest

There are no conflicts to declare.

Acknowledgements

We acknowledge financial support from the Research Council of Norway under the following projects: Hydrogen Storage in Subsurface Porous Media (project no. 325457) and the Centre for Sustainable Subsurface Resources (project no. 331841). We also acknowledge partial funding from the project HyDRA-Diagnostic Tools and Risk Protocols to Accelerate Underground Hydrogen Storage (project no. 101192337). This

project is co-funded by the European Union and supported by Clean Hydrogen Partnership and its members. The authors would like to thank Dr. Malin Haugen for the experimental setup, Dr. David Landa-Marbán for the velocity simulations, Dr. Nicole Dopffel for the microbial expertise in biogeochemical interactions, Ben Heydolph for preparing the bacterial solution culture and Dr. Leif-Erik Rydland Pedersen for assistance with Raman spectroscopy tests.

References

1 W. Song, T. W. de Haas, H. Fadaei and D. Sinton, *Lab Chip*, 2014, **14**, 4382–4390.
2 W. Song and A. R. Kovscek, *Lab Chip*, 2015, **15**, 3314–3325.
3 W. Yun, S. Chang, D. A. Cogswell, S. L. Eichmann, A. Gizzatov, G. Thomas, N. Al-Hazza, A. Abdel-Fattah and W. Wang, *Sci. Rep.*, 2020, **10**, 782.
4 S. S. Datta, I. Battiato, M. A. Fernø, R. Juanes, S. Parsa, V. Prigiobbe, E. Santanach-Carreras, W. Song, S. L. Biswal and D. Sinton, *Lab Chip*, 2023, **23**, 1358–1375.
5 N. S. K. Gunda, B. Bera, N. K. Karadimitriou, S. K. Mitra and S. M. Hassanizadeh, *Lab Chip*, 2011, **11**, 3785–3792.
6 S. Morais, A. Cario, N. Liu, D. Bernard, C. Lecoutre, Y. Garrabos, A. Ranchou-Peyruse, S. Dupraz, M. Azaroual, R. L. Hartman and S. Marre, *React. Chem. Eng.*, 2020, **5**, 1156–1185.
7 N. Liu, A. R. Kovscek, M. A. Fernø and N. Dopffel, *Front. Energy Res.*, 2023, **11**, 1124621.
8 J. W. Grate, R. T. Kelly, J. Suter and N. C. Anheier, *Lab Chip*, 2012, **12**, 4796–4801.
9 V. Berejnov, N. Djilali and D. Sinton, *Lab Chip*, 2008, **8**, 689–693.
10 T. Zhu and M. Dittrich, *Front. Bioeng. Biotechnol.*, 2016, **4**, 4.
11 W. Wang, S. Chang and A. Gizzatov, *ACS Appl. Mater. Interfaces*, 2017, **9**, 29380–29386.
12 S. G. Lee, H. Lee, A. Gupta, S. Chang and P. S. Doyle, *Adv. Funct. Mater.*, 2016, **26**, 4896–4905.
13 D. Le-Anh, A. Rao, S. C. Ayirala, M. B. Alotaibi, M. H. Duits, H. Gardeniers, A. A. Yousef and F. Mugele, *Microfluid. Nanofluid.*, 2020, **24**, 1–12.
14 H. Li, A. Raza, Q. Ge, J.-Y. Lu and T. Zhang, *Soft Matter*, 2020, **16**, 6841–6849.
15 F. H. Y. Lui, L. Xu, P. Michaux, J. Biazik, G. F. S. Harm, R. A. Oliver, P. Koshy, W. R. Walsh, R. J. Mobbs, T. C. Brennan-Speranza, Y. Wang, L. You and C. C. Sorrell, *Nano Sel.*, 2022, **3**, 1321–1336.
16 W. Song, F. Ogunbanwo, M. Steinsbø, M. A. Fernø and A. R. Kovscek, *Lab Chip*, 2018, **18**, 3881–3891.
17 S. Xia, A. Davletshin and W. Song, *Energy Fuels*, 2023, **37**, 14666–14673.
18 M. Buchgraber, M. Al-Dossary, C. M. Ross and A. R. Kovscek, *J. Pet. Sci. Eng.*, 2012, **86–87**, 27–38.
19 B. Benali, *The degree of philosophiae doctor Doctoral dissertation*, The University of Bergen, 2024.
20 B. Benali, A. Sæle, N. Liu, M. A. Fernø and Z. P. Alcorn, *Transp. Porous Media*, 2023, **150**, 427–445.
21 T. O. Okyay, H. N. Nguyen, S. L. Castro and D. F. Rodrigues, *Sci. Total Environ.*, 2016, **572**, 671–680.
22 H. Yoon, K. N. Chojnicki and M. J. Martinez, *Environ. Sci. Technol.*, 2019, **53**, 14233–14242.
23 N. Liu, M. Haugen, B. Benali, D. Landa-Marbán and M. A. Fernø, *Chem. Geol.*, 2023, **641**, 121782.
24 N. Liu, M. Haugen, B. Benali, D. Landa-Marbán and M. A. Fernø, *Int. J. Greenhouse Gas Control*, 2023, **125**, 103885.
25 J. Jimenez-Martinez, J. Nguyen and D. Or, *Rev. Environ. Sci. Bio/Technol.*, 2022, **21**, 27–52.
26 D. V. Okhrimenko, K. N. Dalby, L. L. Skovbjerg, N. Bovet, J. H. Christensen and S. L. S. Stipp, *Geochim. Cosmochim. Acta*, 2014, **128**, 212–224.
27 L. Huang, Y. Jin, D. Zhou, L. Liu, S. Huang, Y. Zhao and Y. Chen, *Int. J. Environ. Res. Public Health*, 2022, **19**, 12191.
28 A. B. Cunningham, R. Gerlach, L. Spangler, A. C. Mitchell, S. Parks and A. Phillips, *Energy Procedia*, 2011, **4**, 5178–5185.
29 D. Landa-Marbán, Open-source image-based framework for computational fluid dynamics on microsystems, **https://github.com/daavid00/pymm**.
30 C. Chang, Q. Zhou, M. Oostrom, T. J. Kneafsey and H. Mehta, *Adv. Water Resour.*, 2017, **100**, 14–25.
31 N. Dopffel, S. Jansen and J. Gerritse, *Int. J. Hydrogen Energy*, 2021, **46**, 8594–8606.
32 A. Al-Yaseri, H. Al-Mukainah, N. Yekeen and A. S. Al-Qasim, *Int. J. Hydrogen Energy*, 2023, **48**, 3583–3592.
33 A. Rezaei, A. Hassanpouryouzband, I. Molnar, Z. Derikvand, R. S. Haszeldine and K. Edlmann, *Geophys. Res. Lett.*, 2022, **49**, e2022GL099433.

